Article

An Optimization-Based Supervisory Control and Coordination Approach for Solar-Load Balancing in Building Energy Management [†]

James Allen [1], Ari Halberstadt [2], John Powers [2] and Nael H. El-Farra [1,]*

1 Department of Chemical Engineering, University of California, Davis, CA 95616, USA; jtallen@ucdavis.edu
2 Extensible Energy LLC., Lafayette, CA 94549, USA; ari@extensibleenergy.com (A.H.); jpowers@extensibleenergy.com (J.P.)
* Correspondence: nhelfarra@ucdavis.edu
† A preliminary version of this work appeared in the Proceedings of the American Control Conference, Boston, MA, USA, 27–29 June 2018.

check for
updates

Abstract: This work considers the problem of reducing the cost of electricity to a grid-connected commercial building that integrates on-site solar energy generation, while at the same time reducing the impact of the building loads on the grid. This is achieved through local management of the building's energy generation-load balance in an effort to increase the feasibility of wide-scale deployment and integration of solar power generation into commercial buildings. To realize this goal, a simulated building model that accounts for on-site solar energy generation, battery storage, electrical vehicle (EV) charging, controllable lighting, and air conditioning is considered, and a supervisory model predictive control (MPC) system is developed to coordinate the building's generation, loads and storage systems. The main aim of this optimization-based approach is to find a reasonable solution that minimizes the economic cost to the electricity user, while at the same time reducing the impact of the building loads on the grid. To assess this goal, three objective functions are selected, including the peak building load, the net building energy use, and a weighted sum of both the peak load and net energy use. Based on these objective functions, three MPC systems are implemented on the simulated building under scenarios with varying degrees of weather forecasting accuracy. The peak demand, energy cost, and electricity cost are compared for various forecast scenarios for each MPC system formulation, and evaluated in relation to a rules-based control scheme. The MPC systems tested the rules-based scheme based on simulations of a month-long electricity consumption. The performance differences between the individual MPC system formulations are discussed in the context of weather forecasting accuracy, operational costs, and how these impact the potential of on-site solar generation and potential wide-spread solar penetration.

Keywords: model predictive control; supervisory control; building energy management; renewable energy forecasting

1. Introduction

With the concerted efforts in recent times aimed at lowering the usage and consumption of conventional energy resources, the use of renewable energy generation and its integration with the grid have been growing. This push towards an aggressive reduction of the carbon footprint of modern living and infrastructure has naturally had a focus on curtailing conventional energy consumption in the larger consuming sectors, i.e., industrial energy use. In this context, the problems of enhancing the energy efficiency of industrial processes and maximizing the energy cost savings in the industrial sector have been the subject of significant research work, especially since small efficiency-enhancing

measures over a single industry can translate into significant large-scale cost-savings. The types of energy savings that can be achieved typically entail solutions that are specific to the type of process under study (e.g., [1]).

With the large-scale potential applications of small local distributed generation systems in both the residential and commercial markets, a significant untapped bed of potential renewable energy generation exists and could significantly reduce the need for conventional energy generation in these sectors. This topic has received significant attention in recent years (e.g., [2–7]). The installation of these local generation systems needs to make practical sense to the local user in order for them to see wide-spread use. This new marked penetration potential, however, is also dependent on the ability of the existing grid infrastructure to handle this large-scale deployment and integration of these small local renewable generation systems (e.g., [8]).

To move toward a more ubiquitous deployment of locally distributed generation in the residential and commercial sectors, and the reduction of conventional energy use that comes with it, the benefits to the local user via energy cost reduction and the benefits to the grid via reduced load need to be simultaneously addressed. Efforts in this direction have largely focused on one side of the problem at a time. For example, a number of studies have looked into ways of characterizing the local energy consumption in buildings with the aid of performance estimation models that help assess energy efficiency and improvement opportunities (e.g., [7,9–12]). The challenges and solutions that arise when modeling non-conventional buildings, such as historical ones, have also been addressed (e.g., [13,14]). A methodological analysis of the local energy use to reduce load demand is important as it enables the development of demand response strategies (e.g., [15]), as well as the development of strategies for peak demand reduction (e.g., [16]).

Beyond characterizing the building's local energy consumption, the actual realization of the benefits of energy cost reduction to the user when the building is integrated with on-site renewable generation requires the development of a local energy management system that balances the load demand with the generation in a way that benefits the user. Energy management strategies range from the use of active energy storage via batteries (e.g., [17]) and purpose-built ice and/or hot water reservoirs (e.g., [18,19]) to the use of more passive storage methods utilizing the thermal mass of the building (e.g., [20]). There has also been extensive work on the development and implementation of improved monitoring and intelligent control systems for energy management in buildings (e.g., [21–24]). These include heuristic approaches for rules-based control schemes; operational optimization of the larger energy load processes, such as climate control, and integrated optimization approaches, such as model predictive control methods, which allow for multi-objective optimization and scheduling of loads to multiple electrical subsystems that influence the building's overall electrical use (e.g., [25–27]).

Rules-based control approaches rely on deterministic policies for determining the operational set-points and energy flows. While these approaches are generally easier to implement, they typically leave only a limited margin for optimization. Model predictive control methods, on the other hand, involve the explicit use of dynamic optimization techniques to determine and adjust the operational set-points in real time based on several inputs such as weather conditions, load and generation data, and external disturbances. These methods tend to exhibit a higher degree of implementation complexity, but can typically achieve substantial savings, explicitly account for occupant comfort into the energy management strategy, and allow for an overall optimization of the energy flows to and from the grid.

Although all of these methods have shown significant promise in the realm of local energy reduction, an examination of the literature shows that results on the large-scale integration of residential and commercial buildings with the grid remain limited at present; thus limiting the prospects of implementing these types of energy saving methods on a larger scale. Specifically, existing optimization-based energy management strategies focus mostly on reducing the cost of electricity to the user, especially when the building is coupled with local renewable energy generation, without

including the impact on the grid in the energy management optimization formulation. The logistics of wide-scale deployment of local renewable sources with their time-dependent stochastic energy generation profiles poses fundamental problems when integrated into the existing grid infrastructure (e.g., [28]). Potential solutions to this quandary include capping the renewable penetration geographically, readjusting the fiscal incentives to make it less attractive, or the implementation of smart-grid solutions (e.g., [29]). Smart-grid solutions, while generally appealing, require increased levels of inter-connectivity and communication between the grid and the grid users. An alternative solution, which promotes the large-scale deployment of local renewable generation without the need for increased levels of communication between the grid and the users, is a more decentralized approach where the generation-load balance is optimized at the local (i.e., building) level in a way that reduces the building's own impact on the grid. This approach is the focus of the current study, and its feasibility is supported by existing results in the literature on the efficacy of policies for peak load reduction in office buildings [16]. This study is particularly relevant to the goal of wide-scale deployment of local renewable generation as it demonstrates the merit of regulating local behavior to impact the grid as a whole.

The problems associated with the wide-scale integration of local renewable generation in residential and commercial buildings can be illustrated by looking at the case of a financially motivated user installing on-site renewable generation (e.g., rooftop solar). Fiscal savings associated with decreased energy use are often coupled with the potential revenue of selling excess power back to the grid. This is done when on-site power generation exceeds the local demand, or when it is financially advantageous to sell on-site generated power due to time-of-use pricing. While this may prove to be an attractive option for a single user, due to the additional income and increasing the attractiveness of on-site generation, one can see how if a substantial number of users are trying to sell electricity back to the grid at the same time of the day, then the supply-demand dynamics would start to breakdown. Such a situation can be seen when there is a drastic increase in local solar generation from users in a geographic area; this naturally leads to a reduction in demand from the generation side during the daylight hours but not in a predictable manner.

Owing to the intermittent and stochastic nature of solar power generation, the availability of solar power is not fully predictable, even though the long-term trends of solar irradiance seem to be generally stable. Many buildings with on-site solar power generation do not typically take the time-varying nature of solar generation into account when implementing building controls and load scheduling. This typically leads to increased fluctuations in the power demand of the building from the grid, even if the net volume of power is reduced. This type of behavior is likely somewhat trivial to the user as the peak load is not reduced and the on-site generation helps lower the overall energy consumption and thus increase the financial savings to the user. However, the increased fluctuations in load demand pose significant challenges to the grid itself, especially as the power needs of the grid users become less predictable. From the grid perspective, it would be advantageous if buildings with on-site renewable energy generation interfaced with the grid in a way that allows load-generation coordination in a more predictable manner. Such an approach would potentially help achieve increased levels of renewable penetration without negative ramifications for grid operations.

Motivated by these considerations, we focus in the present work on the problem of mutually-advantageous scalability of local on-site solar power generation in grid-interfaced commercial buildings. The key idea is to maximize the on-site power generation and usage while at the same time reducing the impact on the grid by optimally managing the solar generation-load balance at the local building level. The underlying premise of this approach is the fact that it would be advantageous if each grid-connected building were to minimize its own grid impact independent of other grid users. This represents a decentralized solution to the mitigation of the grid impact problem and would enable the large-scale integration and deployment of local on-site renewable energy generation, while at the same time keeping the collective demand on the grid to a minimum. This decentralized approach is appealing in that it promotes the scalability goal (with its associated

economic and environmental benefits) without the need for increased levels of inter-user or user-grid communication or coordination.

To realize this goal, an optimization-based supervisory control and coordination strategy based on the principles of model predictive control (MPC) is developed and implemented for the energy management in a simulated commercial building with flexible energy loads, on-site solar power generation and battery storage. The flexible electrical loads include Heating Ventilation and Air Conditions (HVAC) use, Electric Vehicle (EV) charging, lighting and other miscellaneous loads. The supervisory MPC system leverages the flexible nature of the building loads throughout the day, taking into account solar forecasting in an effort to reduce the total electricity cost to the user while easing the load demand on the grid.

The efficacy of this strategy is evaluated using various MPC formulations in an effort to balance on-site generation with building load with the goal to reduce peak usage and lower overall energy cost for the user. The following three objective functions are considered for the MPC formulations, including minimizing the peak load demand, minimizing the net energy use, and minimizing a weighted sum of these two measures. The resulting MPC formulations are tested on the simulated building with both perfect and imperfect weather forecasting integrated into the MPC system. This is done for both a single day and a month-long trial. The energy cost, peak load demand and total cost (when applicable) are reported for these time frames and referenced with a rules-based energy management scheme for context. From the user's standpoint this framework will result in a monthly reduction in peak demand charges as well as a reduction in electricity cost. From the grid's perspective a more consistent load will be drawn by the user resulting in increased longevity of equipment, higher operational efficiency, and increased predictability leading to a win-win scenario. With the deployment of this framework for building energy management where both the grid impact and cost from the local user's standpoint are accounted for, the path for far more substantial utilization of solar energy on a grand scale is clearer.

2. Building Description: A Motivating Example

While the local deployment of solar energy generation systems on-site can be used to reduce the cost of grid electricity usage to the user, it does little to reduce the strain of peak demand on the grid, and may in fact exacerbate the problem when on-site generation is deployed on a wide scale. The lack of peak demand reduction is problematic for both the electricity end-user and the grid. A high peak demand implies that high power needs to be supplied by the gird for short periods of time, and that a premium in peak demand charges must be paid for this convenience by the user. Conventionally, the fees paid by mid-tier energy users over a single billing cycle include a fee related to their highest peak usage (billed by the kW) and a fee for the cumulative use of energy over the same period. For the purposes of this study, we consider a price of $17.04/kW for the peak use, and a price of $0.14–$0.22/kWh for the cumulative use depending on the time of day [30].

It is common for moderate-sized office buildings to find themselves in this pricing and usage scheme, and these same buildings are also ideal candidates for solar integration due to their relatively large roof area. Moreover, any user would desire to increase the cost-savings that any renewable generation integration would provide. It is this type of general case that motivates the research here. By choosing appropriate objective functions for a building energy management system based on energy use and peak demand, a mutually beneficial operation can potentially be achieved between the user and the grid. This hinges on the chosen objective functions acting as adequate surrogates for capturing the interplay between the financial cost to the user, on the one hand, and the impact of the user on the grid, on the other. By minimizing the net energy usage and peak demand, the user benefits from a reduced bill, and by minimizing the peak demand, grid operations benefit from a more level, more predictable and less volatile load profile.

In this work, and as a simulation test-bed for the development and implementation of the supervisory MPC system to be proposed, we consider an office building with three stories in

Merced, California. The building has 150,000 square foot of area and 750 occupants that occupy the building between 08:00 and 18:00. Further details on the building location and definition are given in Appendices A.1 and A.2. The building is connected to the grid but also includes rooftop solar panels for on-site power generation. The loads considered include an electric vehicle (EV) charging stations, an HVAC system, dimmable lights, and various miscellaneous loads. Battery storage is also assumed to be available. A supervisory MPC system is integrated into the building energy management system to optimally coordinate the energy generation and/or consumption of the various component subsystems, with objective functions that reasonably minimize the impact on the grid as well as the electricity cost to the user. Three different objective functions are considered here, and include the net energy use, the peak load demand, and a weighted sum of the energy use and peak load demand.

The resulting MPC systems are implemented on the simulated building with the aid of a forecasting scheme that predicts the availability of solar power based on the relevant weather and environmental parameters. Scenarios involving both accurate and inaccurate forecasting are considered and analyzed. Perfect forecast simulations are carried out using historical data for the simulated building's solar generation and environmental parameters available from [31,32], while imperfect forecast simulations combine the historical data with an augmented clear sky model [33] to generate the predictions. This clear sky model is augmented to best fit the historical data available and this fit is corrected in real time through the use of a moving-horizon estimation scheme. The impact of forecast accuracy on the various metrics of energy cost, peak demand, and total electricity cost (as calculated by the PG&E A-10 rate [30]) is assessed, and referenced against an intelligent rules-based energy management scheme.

In the remainder of this section, we briefly describe the component subsystems considered in the building, and provide an overview of the corresponding models used in the MPC system implementation. The details of all the component models, as well as the assumptions made in those models, can be found in Appendix A. The model equations were coded into MATLAB, which was used to conduct all the necessary optimization and simulation scenarios (see Section 4).

2.1. On-Site Energy Generation: Photovoltaic (PV) Panels

We consider rooftop solar panels on half of the available usable area leading to a AC maximum generation capacity of 154 kW. The available power at a given time is estimated from the following relation:

$$P_{pv}(t) = I_{incident} \cdot A \cdot \eta(T), \tag{1}$$

where $P_{pv}(t)$ is the usable power available from the solar array at time t, $I_{incident}$ is the solar irradiance which is obtained from [32], A is the effective total area of the arrays, and $\eta(T)$ the efficiency of conversion to usable power, which is a function of temperature, T, and dependent on the efficiency of the solar panel, and the inverter. Further details on the modeling equations and assumptions for PV electricity generation are given in Appendix A.3.

2.2. Battery Storage

A key component of any energy management system is an energy storage system that can be charged to store the excess power available from renewables at certain times of the day, and can then be discharged to meet the load demands (if necessary) at other times. In this study, we consider a battery storage system with a capacity of 50 kWh, and with 92% charge/discharge efficiency and a

25% minimum charge. The following simple state of charge model is used to estimate the charge of the battery:

$$C_b(t + \Delta t) = C_b(t) + P_b(t) \cdot \Delta t \cdot \eta_b$$

$$s.t.$$

$$C_{b\ \min} \leq C_b(t) \leq C_{b\ \max}$$

$$\Delta C_{b\ \min} \leq C_b(t + \Delta t) - C_b(t) \leq \Delta C_{b\ \max} \tag{2}$$

where $C_b(t)$ is the charge of the battery at time t, P_b is the power reference to the battery, and η_b is the charge/discharge efficiency of the battery. According to this model, the battery charge at a given time is the sum of the charge at the previous time and the battery's power reference at the previous time corrected for charging and discharging inefficiencies, which are functions of the power set-point. Of note in this model is the consideration of constraints on (1) the minimum and maximum battery charge levels, i.e., ($C_{b\ \min}$ and $C_{b\ \max}$), and (2) the rate of charge, ($\Delta C_{b\ \min}$, $\Delta C_{b\ \max}$), which are imposed to ensure battery longevity and incorporate safety considerations.

2.3. Building Loads

The building loads considered in the working model include an HVAC system, EV charging stations, dimmable lighting and miscellaneous other loads.

2.3.1. Heating Ventilation and Air Conditioning (HVAC)

We consider an HVAC system with a capacity of 200 kW, with an allowable temperature range of 20–24 °C when the building is occupied (between 08:00 and 18:00), and an allowable temperature range of 18–27 °C when the building is unoccupied. For the sake of a simple illustration of the energy management strategy, we consider here a simple model of the HVAC system based on an energy balance. The energy balance accounts for the solar irradiance and ambient temperature on the outside of the building, and also includes the internal heat generation inside the building from the occupants and from electrical loads. The model also includes an efficiency factor that captures the HVAC system's ability to counteract the overall heat inflow into the building. The dynamics of the building temperature are represented by the following energy balance:

$$m \cdot c_p \cdot \frac{dT}{dt} = \dot{Q}_{generation} + \dot{Q}_{envelope} + \dot{Q}_{ventilation} + \dot{Q}_{HVAC}$$

$$s.t.$$

$$T_{\min}(t) \leq T(t) \leq T_{\max}(t) \tag{3}$$

where $\dot{Q}_{generation}$ is the rate at which heat is generated inside the building (i.e., from warm bodies, heat generation from electronics, etc.), $\dot{Q}_{envelope}$ is the rate at which external heat is transferred to the building from the surroundings into the building envelope (i.e., solar heating, heat transfer from ambient air, etc.), $\dot{Q}_{ventilation}$ is the heat energy needed to treat the outdoor air to maintain indoor air quality, and $\dot{Q}_{HVAC}$ is the heat load removed by the HVAC system. The minimum and maximum allowable temperature, $T_{\min}$ and $T_{\max}$, are dictated by the comfort level, and depend on the occupancy status of the building. Further details on the breakdown of each of the components in the above energy balance, along with the modeling equations and assumptions, are given in Appendix A.4.

2.3.2. Electric Vehicles (EV) Charging Stations

To model the contribution of EV charging to the building load, we consider 10 EVs with 7.4 kWh capacity each. The EVs are assumed to arrive at a 25% charge level at 08:00 and a 90% target charge

level at 18:00, and are used with a 92% charge efficiency. The EVs are essentially treated as batteries that cannot be discharged, as follows:

$$C_{ev}(t + \Delta t) = C_{ev}(t) + P_{ev}(t) \cdot \Delta t \cdot \eta_{ev}$$
$$s.t.$$
$$C_{ev}(t + \Delta t) \geq C_{ev}(t)$$
$$C_{ev\,\min}(t) \leq C_{ev}(t) \leq C_{ev\,\max}(t)$$
$$C_{ev}(t + \Delta t) - C_{ev}(t) \leq \Delta C_{ev\,\max} \tag{4}$$

where $C_{ev}(t)$ is the charge of the EV at time t, $P_{ev}(t)$ is the power sent to the EV at time t for a duration of Δt, η_{ev} is the EV charging efficiency. The time-dependent minimum and maximum charge constraints are denoted by $C_{ev\,\min}(t)$ and $C_{ev\,\max}(t)$, respectively.

2.3.3. Lighting

We consider a simple model of the illuminance of the lighting system as follows:

$$L(t) = P_l(t) \cdot \eta_l$$
$$s.t.$$
$$L_{\min}(t) \leq L(t) \leq L_{\max}(t) \tag{5}$$

where $L(t)$ is the illuminance at time t, $P_l(t)$ is the power at time t, and η_l is the efficiency of the light bulbs used. Time-dependent minimum and maximum illuminance constraints, denoted by $L_{\min}(t)$ and $L_{\max}(t)$, are imposed for workplace comfort, and a time-dependent schedule based on building occupancy is used to determine the lower and upper bounds. For the purpose of this study, an efficiency of 90 lumens per watt is assumed, and a 500 lux target for workplace lighting with a 400 lux minimum are considered. The maximum and minimum illuminances are enforced during the building occupancy hours (from 8:00 to 18:00), and are set to zero when the building is unoccupied. It should be noted that the illuminance effects of daylight are not considered here. All illuminance is assumed to come from the interior lighting to meet the lighting standards mentioned. Further details regarding the specifics of the lighting system assumptions are given in Appendix A.5.

2.3.4. Miscellaneous Loads

To represent other building loads, such as plug loads, elevators, and other electrical loads, a schedule-dependent set of constant values based on the building's occupancy status is used for these loads throughout the day. While these loads can generally be varied in a more stochastic manner, they are chosen to be constant in this study to simplify the viewing of the results. A description of the miscellaneous load assumptions is given in Appendix A.5.1.

3. Optimization-Based Building Energy Management

The overarching goal of this work is to develop an energy management strategy that minimizes the total cost of electricity to the user while simultaneously minimizing the load on the grid. The formulation of an objective function that captures this goal, naturally, needs to include metrics that represent the effects on both the user and the grid. From the grid's perspective, an ideal load profile would be a uniform flat line with constant low demand. This type of demand is simple for the grid operators to predict and dispatch power to meet. This idealized load profile would also exhibit the lowest feasible peak load since there would be no peaks per se. A low peak demand is certainly desirable from the end user's perspective as it would reduce the peak demand charge. This is to be understood with the caveat that the constant load is not unreasonably large so as to avoid large energy costs. With these considerations in mind, three different objective functions are chosen in Section 3.1

to devise an optimization-based supervisory control structure that coordinates the building's energy management strategy. The supervisory control structure is then applied to the simulated building and evaluated for efficacy in Section 4.

The implementation of the supervisory control structure is done through interfacing it with an existing building control system, as shown in the schematic diagram of Figure 1. In this setup, all systems requiring electrical loads (HVAC, EV, Lighting, and Battery storage) are sent power set-point references and their outputs of interest (temperature, state of charge, illuminance, and state of charge, respectively) are reported back to the supervisory controller. The PV subsystem operates independently and, for simplicity, is assumed to supply the maximal available solar power to the building at all times. This can be realized through the use of maximum power point tracking controllers, where the power output is calculated as depicted in Equation (1). The PV-generated power as well as the HVAC system are both affected by environmental factors, with the PV being dependent on the solar irradiance, and the HVAC system being impacted by the exterior climate conditions.

The supervisory MPC receives the states of the individual subsystems through the building interface at a certain pre-determined frequency (every 15 min in the simulation case studies). Using the predictions of the internal models of the component subsystems embedded within the control structure, the MPC solves a finite-horizon optimization problem to determine the trajectory of optimal power set-points for the controllable subsystems over a certain future horizon (5 h in the simulation case studies). The optimal trajectory is obtained by minimizing the objective function of interest, subject to the appropriate constraints, and the computed optimal set-points for the next 15-min window are then transmitted to the building subsystems for implementation (through local regulatory controllers) and the process is repeated in a receding horizon fashion.

The plug-and-play nature of this supervisory control structure, with its modular subsystem interface, is intended to facilitate future deployment and incorporation of more advanced models than the proof-of-concept type models considered in Equations (2)–(5) with ease. The design of this kind of MPC-building communication interface enables integration into existing building control systems with an eye towards implementing the proposed MPC system on existing buildings.
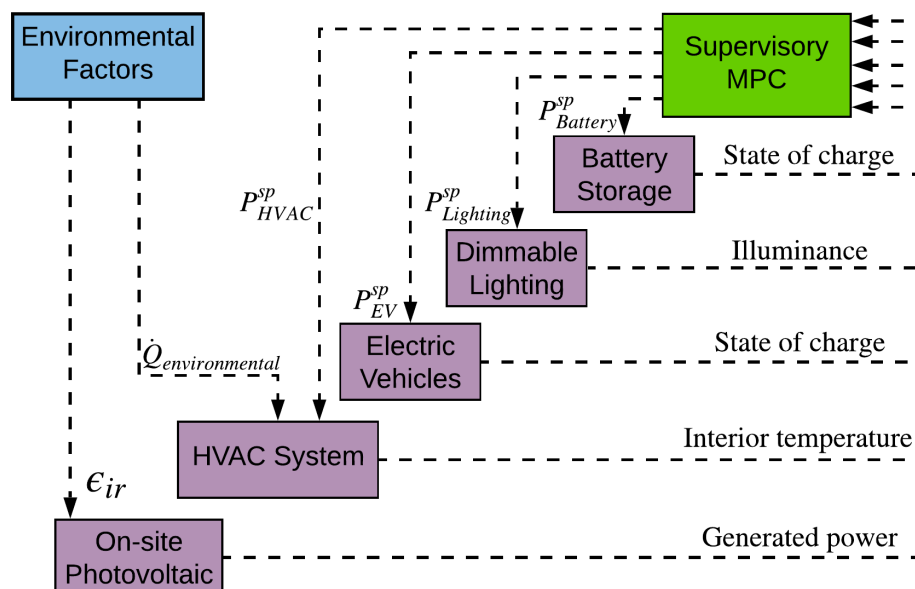

Figure 1. Supervisory control, optimization and coordination structure.

3.1. Problem Formulation

To achieve the goal of minimizing grid load and electricity cost to the user, we must first create objective ways to measure these metrics. To this end, we consider three different objective functions

in the formulation of the supervisory MPC system. The first objective aims to minimize the net load. This is called the "Net Energy Use" (NEU) objective and is given by:

$$J(P_i^{sp}) = \sum_{k=t}^{t+N \cdot \Delta t} \left| P_{\text{total}}(k) \right| + \sum_i \left(w_i \cdot \sum_{k=t}^{t+N \cdot \Delta t} \|\text{Ref.}_i - \text{Traj.}_i\| \right) \tag{6}$$

where $P_i^{sp} = [P_{EV}^{sp}(k), P_{HVAC}^{sp}(k), P_{Lighting}^{sp}(k), P_{PV}^{sp}(k), P_{Battery}^{sp}(k)]$, $P_{\text{total}}(k) = \sum_i P_i^{sp}(k)$, P_i^{sp} is the power set-point for subsystem i, N is the prediction horizon length and Δt is the update period. The above objective function includes an additional penalty on the deviation from a pre-defined target trajectory for each subsystem, with a penalty weight w_i. This penalty is introduced in order to "guide" the solution of the optimization problem without the horizon length being overly large. This leads to an augmented rules-based control strategy where the MPC has the extra flexibility it needs to adjust power allocations among the component subsystems so as to meet the objective function. An example of such penalty is a penalty on deviating from a pre-defined linear charge target trajectory for the EV subsystem (see Section 4 for an illustration). The MPC formulation corresponding to the objective function in Equation (6) is referred to as the "Net Energy Use" MPC (or NEU MPC for short).

The second objective considered in this work aims to minimize the peak load demand. This is called the "Peak Demand" (PD) objective and is given by:

$$J(P_i^{sp}) = \max_{k \in [t, t+N \cdot \Delta t]} \left(P_{\text{total}}(k) \right) + \sum_i \left(w_i \cdot \sum_{k=t}^{t+N \cdot \Delta t} \|\text{Ref.}_i - \text{Traj.}_i\| \right) \tag{7}$$

The MPC formulation with this objective function is referred to as the "Peak Demand" MPC (or PD MPC short). The third objective function seeks to minimize a weighted sum of the net energy use and the peak demand load as follows:

$$J(P_i) = \alpha \cdot \sum_{i=t}^{t+N \cdot \Delta t} \left| P_{\text{total}}(i) \right| + \beta \cdot \max_{i \in [t, t+N \cdot \Delta t]} \left(P_{\text{total}}(i) \right) + \sum_i \left(w_i \cdot \sum_{k=t}^{t+N \cdot \Delta t} \|\text{Ref.}_i - \text{Traj.}_i\| \right) \tag{8}$$

where α and β are the weighting factors on each of the terms in the composite weighted sum objective function. This objective referred to as the "Weighted Sum" objective, and the corresponding MPC formulation is referred to as the "Weighted Sum" MPC (WS MPC for short).

It should be noted that, for each MPC formulation, the objective function is to be minimized subject to the constraints represented by Equations (2)–(5), as well as an additional ad hoc penalty for the EV subsystem that accrues penalties for deviations from a pre-determined linear charge target trajectory. The added penalty guides the optimization of the EV subsystem charging profile to meet the end of day charge state without the need for a large horizon.

It is also worth noting that, unlike conventional formulations for economic optimization that seek to achieve explicit cost minimization, financial cost to the end user is not explicitly considered in the objective functions referenced above. The rationale for this choice is the fact that the energy cost is directly related to the energy use, and therefore one can use the latter as an appropriate surrogate to minimize the fiscal cost to the user (see, for example, [24]). In the same vein, peak load demand can be viewed as a suitable surrogate to both the grid impact and the fiscal cost to the user (in the case of demand charges). In general, demand charges are designed to encourage electricity users to manage the peak power draw by charging users a premium for the peak power used in a monthly billing cycle. Peak demand charges are based on the logistics and infrastructure needs for the deployment and delivery of such large volumes of energy over a short period of time. Due to these considerations, peak use is viewed as an appropriate (though indirect) measure of the user's impact on the grid.

4. Simulation Results

4.1. Base Case: A Rules-Based Energy Management Scheme

In order to assess and compare the effectiveness of the optimization-based control and coordination schemes, a rules-based control scheme that relies mostly on intuition was developed and used as a base case for reference. This base case scheme involves no optimization and no coordination between the loads, the generation, and the storage subsystems. The following rules describe the implementation of the rules-base control scheme:

- The building's indoor temperature must be maintained by the HVAC subsystem within the same operating bands enforced by the MPC system. The operating band when the building is occupied is 20–24 °C, and 18–27 °C when the building is unoccupied.
- The building's indoor temperature should be kept within one degree of the set-point. The set-point is kept higher while the building is unoccupied, and is reduced one hour prior to the onset of building occupation in order to pre-cool the building.
- The lighting systems are maintained at the target illuminance (500 lux).
- The battery is charged during the off-peak pricing hours, and is discharged during peak pricing hours.
- The EVs are charged at a constant rate to achieve a 90% charged state by the end of the workday after arriving at 25% charged state.

Figure 2 is a load profile plot for the building under the rules-based control scheme. The total building load in black is shown along with the various individual subsystems contributing to the overall building load. It can be seen that the main contributor to the total building load is the HVAC subsystem, and that the net building load reaches a peak near the end of day as the solar generation drops off and outdoor temperature stays high.

In Figure 3 the indoor and outdoor temperatures of the building can be seen, together with the set-point and bounds for the HVAC subsystem. For the start of this specific day the outdoor temperature is cool enough to not warrant any cooling prior to the start of the day even though the temperature set-point drops one hour before the building becomes occupied. It can be seen that as the building becomes occupied the indoor temperature rises until the HVAC system reaches the maximum temperature bound at which point it turns on to keep the indoor temperature at the set-point throughout the day. At the end of the day there is a slight dip in the indoor temperature as the internal heat generation drops as the building becomes unoccupied and internal generation is reduced. The temperature then proceeds to drift by one degree above the unoccupied set-point and the HVAC unit turns on to cool the building. As noted before, the outdoor temperature reaches its peak at around 15:00 and stays fairly high until after the building occupants have left at 18:00 (with the exception of a cloud that shades the building around 16:00). This results in the peak building load occurring late in the day as solar generation dwindles and the need for building cooling remains high.
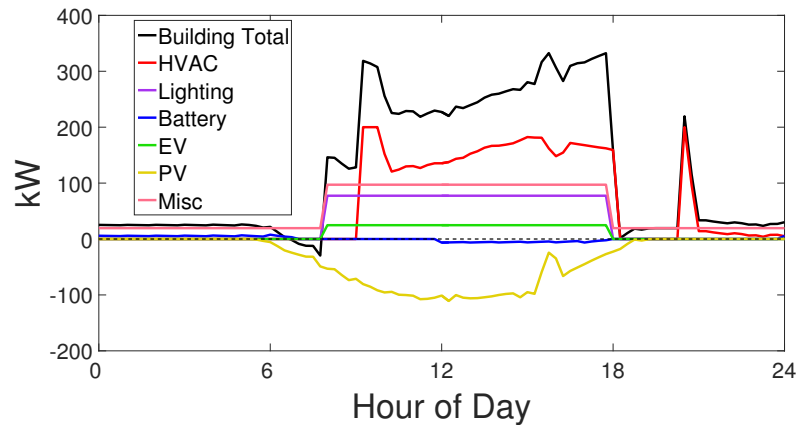
Figure 2. Power consumption profiles for the building and the individual subsystems under rules-based control scheme over a 24 h period.
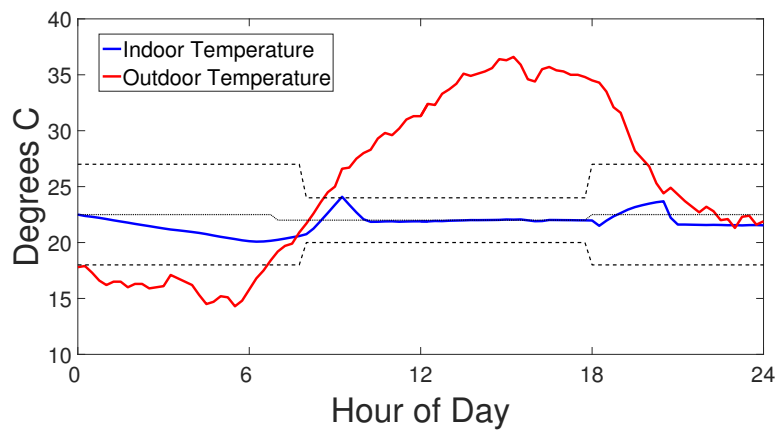

Figure 3. Time profiles of the building's indoor and outdoor temperatures under the rules-based control scheme.

Figure 4 shows the state of charge for the battery storage of the building as well as the electric vehicles. It is clear that the battery follows the preset rules and charges overnight while electricity is cheap and discharges during the peak usage time of the day. The EVs have a linear charge profile to meet the condition of 90% charge by the end of the workday at 18:00. This liner charge profile was selected as it provides the smallest demand charge on the building in this rules-based framework.
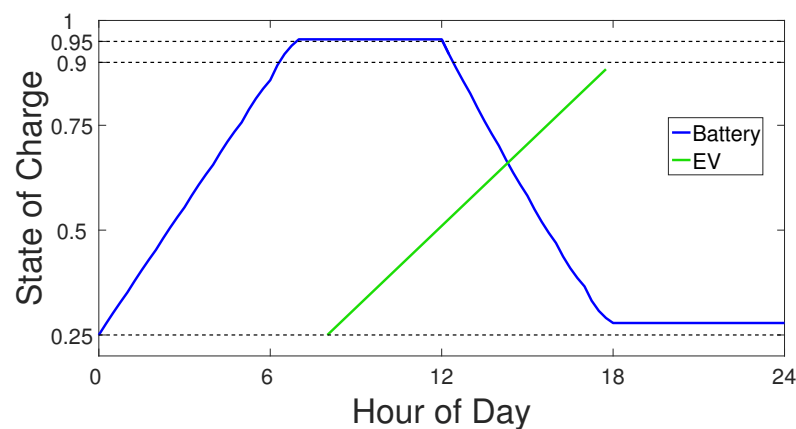

Figure 4. State of charge for the battery storage and electric vehicle (EV) system under the rules-based base case.

4.2. Supervisory MPC Implementation with Perfect Forecasting

Due to the supervisory nature of the MPC system, the component subsystem loads can be coordinated to best meet the optimization objective by leveraging the ability to relax any or all subsystem set-points within the prescribed bounds. The underlying working mechanism is to optimally coordinate the use of electrical energy storage via the battery, the thermal energy storage by pre-cooling the building, and through intelligent charging of the EVs.

To ensure satisfactory operation through minimizing the objective function cost as well as following the prescribed operational limits of the subsystems, it is critical to incorporate the anticipated solar exposure throughout the day as the cost-saving measures are dependent on the solar availability for both power generation and predicting HVAC loads. In the best case scenario, the MPC system would be able to incorporate a perfect forecast of solar availability into the optimization. The resulting performance would be the best performance that the MPC scheme can be expected to achieve.

Figure 5 illustrates the difference in solar power availability from the on-site PV arrays throughout a day, based on both historical solar data [32], and the predictions of an idealized model [33] (called the clear sky model) forecasting the solar irradiance. It can be seen that for this day the predictions of the clear sky model track closely with the actual output of the PV arrays until about mid-afternoon where there is a sharp decrease in the actual solar power generated followed by a diminished generation after this event. This day will be referred to in the simulation case studies to be presented later as the "high solar" day. The key characteristic of this day is the fact that the solar power output predicted by the clear sky model matches well with the actual solar power output based on historical data, suggesting that the sky was likely clear for a large part of this day.
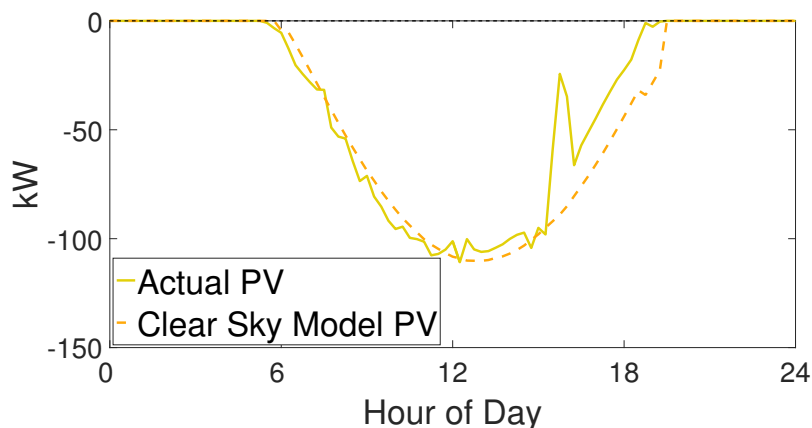

Figure 5. A comparison between actual photovoltaic (PV) power availability (solid line) and the power predicted by the clear sky model (dashed line) for a simulated day with high solar irradiance (29 June 2015).

Figure 6 depicts a simulated day where the actual solar power available based on historical data is substantially less than the predicted solar availability based on the clear sky model. This day will be referred to in the simulation case studies later as the "low solar" day. The substantial discrepancy characterizing this day suggests that the prevalent conditions on that day are those of overcast weather. The "low solar" day represents an important case to investigate the impact of forecast accuracy on the proposed energy management strategy. On a "low solar" day the MPC system would benefit from the use of an accurate forecasting scheme to estimate the solar power availability.
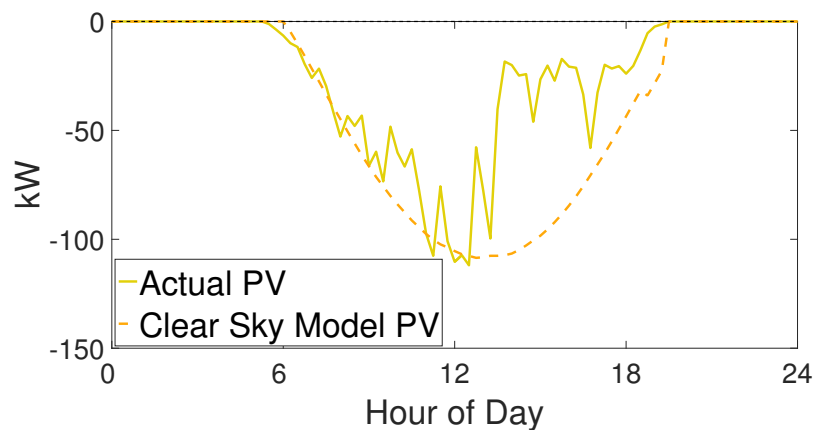
Figure 6. A comparison between actual PV power availability (solid line) and the power predicted by the clear sky model (dashed line) for a simulated day with low solar irradiance (1 July 2015).

Implementation during a "High Solar" Day

Figure 7 depicts the building's power load profiles when the Peak Demand MPC strategy is implemented. Shown in this plot is a contrast between the total building load under this MPC strategy and the resulting load profile when the rules-based control scheme is applied (dashed line). Also shown in the same figure are the power load profiles associated with the building's individual subsystems under the MPC coordination strategy. It is evident that, relative to the base case load profile, the total building load under the MPC strategy is much flatter over the day. The flatter load profile is a direct consequence of the ability of the supervisory MPC system's to curb the component subsystems' loads (mainly that of the HVAC subsystem) at the end of the day as the availability of solar power is diminished.
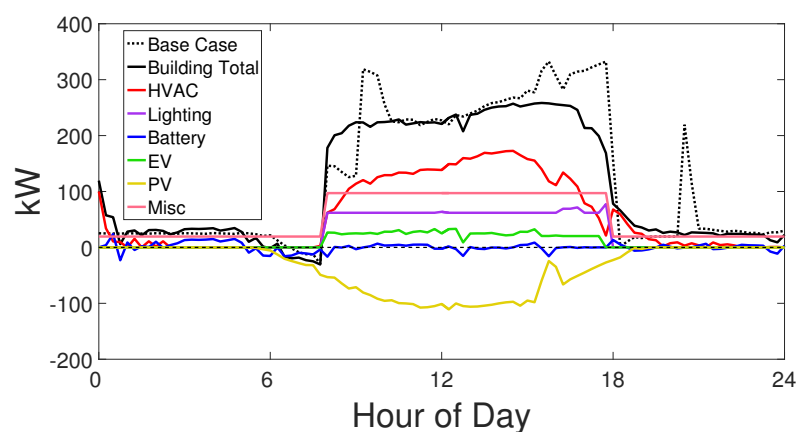

Figure 7. Power usage profiles for the whole building and for the individual subsystems during a "high solar" day under the Peak Demand model predictive control (MPC) with a five-hour horizon and perfect solar forecasting. The dashed profile represents the total building load under the rules-based control scheme.

It should be noted that, due to the availability of a perfect solar forecasting scheme in this simulation scenario, the MPC system is able to respond effectively to the sudden outage in solar power availability taking place around 16:00. The response of the MPC system consists of curtailing the HVAC subsystem's power, dropping the EVs' charging rate, and discharging the battery. As a result of these actions, the total building load experiences remains relatively flat and experiences no significant perturbation during this event.

Figure 8 gives a glimpse into the inner workings of the supervisory MPC and rules-based strategies in terms of their ability to leverage the operational bounds presented with regards to the HVAC subsystem. The temperature profile under the rules-based case shows that the indoor building

temperature is maintained at a steady value throughout the day and remains within the specified bounds. The supervisory MPC strategy with perfect forecasting, however, spends most of the day at the extreme limits of the allowable temperature values, leveraging all the available temperature range to drive total energy cost down. By keeping the temperature at the lower end of the limit during the bulk of the workday, the system can let the temperature drift higher during the end of the day when the on-site solar generation ceases. This behavior can be viewed as some sort of thermal capacitance whereby energy is stored in the form of a cooler building temperature and released when advantageous. This more aggressive management of the building's indoor temperature by the MPC strategy is evident in Figure 7 when comparing the total load near the end of the day with that under the rules-based control scheme.
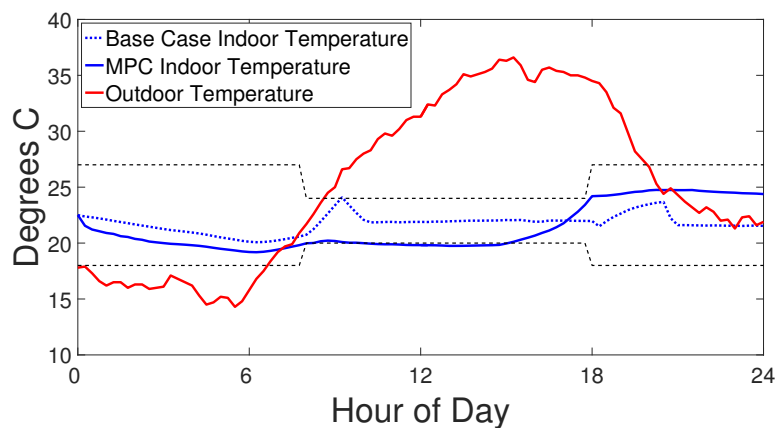

Figure 8. Indoor building temperature profiles under the rules-based control scheme and under the supervisory Peak Demand MPC with perfect forecasting, with upper and lower indoor temperature bounds (dashed black line), referenced with the ambient outdoor temperature.

In Figure 9, the differences in power management are seen for the EV and battery subsystems. It can be seen that the electric vehicles behave in a similar manner for both schemes, with the supervisory MPC affording more flexibility in the charging schedule (as was mentioned in Section 3.1). However, when it comes to the battery the behavior is starkly different for the control strategies compared in the figure. The behavior of the battery is more volatile in the MPC case and undergoes its primary charge and discharge closer together and earlier in the day relative to the base case. This behavior, in conjunction with the results in Figure 7, appears to show that the battery is discharging in an attempt to offset the unoccupied building load prior to the start of occupancy. Likewise, the battery partially charges and discharges multiple times throughout the day to aid in the smoothing of the building load, and in doing so, reducing the peak power draw and buffering some of the fluctuations that the grid would typically see. This can be most clearly seen at one of the sharpest discharge cycles of the day around 16:00 corresponding to the sharp reduction in available solar power.

The results analyzed thus far have been obtained using the Peak Demand MPC as the building's energy management strategy. To examine the impact of the choice of objective function in the supervisory MPC on the building load profile, the total building load under the Peak Demand MPC is compared in Figure 10 with the resulting load profiles under the Net Energy Use MPC, the Weighted Sum MPC and the rules-based management scheme. It can be seen that some subtle differences in the total building load exist between the different MPC strategies. For example, the MPC strategy that aims to minimize the energy use appears to result in more fluctuations in the load profile. This behavior is likely due to the fact that this management strategy is able to offset possible load spikes with troughs while still maintaining the same net load value. By contrast, the MPC strategy that seeks to minimize the peak demand leads to a relatively smoother load profile, consistent with the expectation of a minimal peak value for a flat line. Compared with these two strategies, the Weighted Sum approach appears to split the difference between the other two, depending on the weighting placed on each part of the objective function.
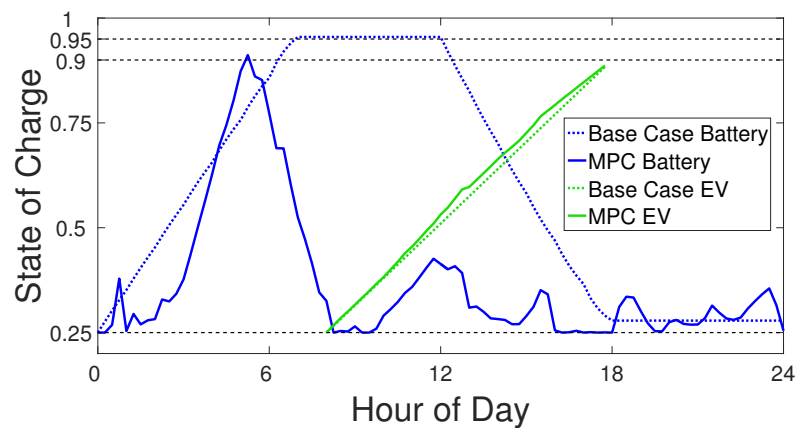
Figure 9. Typical state of charge for the battery storage and EV subsystems under the supervisory MPC system, referenced with the state of charge for the same subsystems in the rules-based base case.
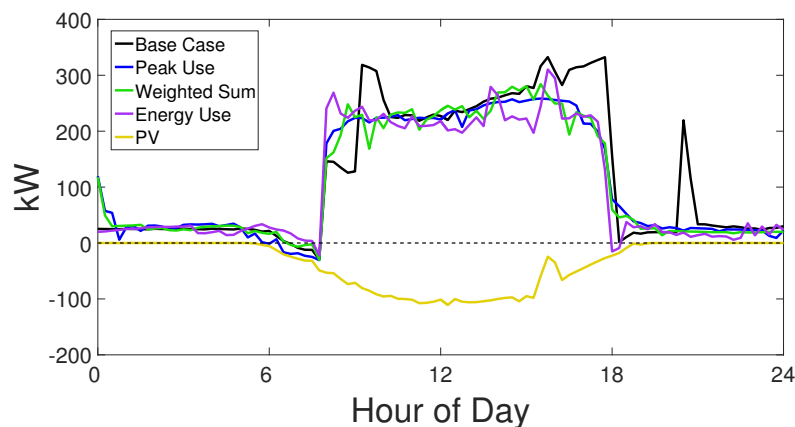

Figure 10. A comparison between the total building load profiles obtained under the rules-based control scheme (black line), the Peak Demand MPC (blue line), the Net Energy Use MPC (purple line), the Weighted Sum MPC (green line), all with perfect solar forecasting and a horizon length of 5 hours, for the "high solar" day. The solar power generation profile is indicated by the yellow line.

4.3. Supervisory MPC Implementation under Imperfect Forecasting

The ease of implementing the clear sky model [33], owing to the fact that it qualitatively captures the correct shape of the solar power profile and the fact that its predictions can be calculated a priori, motivates its use as the underlying forecast method for the solar power availability. To address the imperfect forecasting problem, we use in this section a moving horizon estimation scheme as a way of augmenting the clear sky model predictions and implementing a technically realizable solar forecasting scheme. The key idea is to modify the clear sky model forecast using a constant multiplier at each time step. The value of the constant multiplier is calculated and updated at each time step based on the discrepancies between the measured solar irradiance and the predictions of the clear sky model over some past (rolling) horizon. The modified clear sky model predictions are then used to generate the forecasts of the of available solar power, which are used by the supervisory MPC system.

It should be noted here that, as is the case with any moving horizon estimation scheme, the accuracy of the resulting forecast is generally dependent on the choice of the length of the past moving horizon. In practice, and owing to the relatively short time-scale over which solar irradiance can vary, shorter horizon lengths are expected to favor improved forecast performance. When a discrepancy in the generated solar power is observed at some time, future estimates of the available solar power are then adjusted quickly to compensate for the observed deviation. While this may cause the available solar power to be underestimated in the case of longer forecasts and low values of the

current solar irradiance, it is found in practice that the faster response yields better performance than a slower, more smoothed, response resulting from a longer horizon.

4.3.1. Implementation during a "High Solar" Day

In this part, we apply the supervisory MPC strategies for the same "high solar" day considered in Section 4.2, but with the added moving horizon estimation scheme in place to estimate solar power availability as discussed above.

Figure 11 is analogous to Figure 10 but with the added moving horizon solar forecast information. The figure depicts and compares the load profiles obtained under the rules-based control scheme and under the three supervisory MPC schemes. The trends and analysis here are similar to those observed in Figure 10, with the Net Energy Use MPC exhibiting lower energy use but similar peak demand when compared to the rules-based scheme (in both cases the load peaks at the solar power drop taking place around 16:00). Likewise, the load profiles stemming from the Peak Demand and Weighted Sum MPC formulations appear visually "flatter" than the others, and both exhibit a reduction in peak load demand (notice that the peak still takes place during the solar drop event).
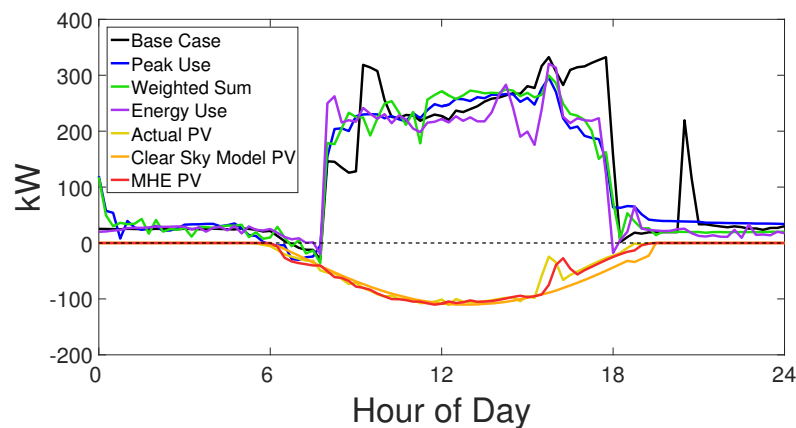

Figure 11. A comparison between the total building load profiles obtained under the rules-based control scheme (black line), the Peak Demand MPC (blue line), the Net Energy Use MPC (purple line), the Weighted Sum MPC (green line), all with a fifteen-minute moving horizon solar forecast and a five-hour MPC horizon for the "high solar" day. The actual solar power availability is shown by the yellow profile; the clear sky model predicted solar power by the orange profile, and the estimated solar availability based on the moving horizon estimation scheme by the red profile.

The different behaviors exhibited by the different MPC formulations are intimately tied to the different optimization strategies they employ. Specifically, the Net Energy Use MPC strategy acts to reduce the building load prior to the solar power drop event, but has limited flexibility or means of compensation in the individual subsystems. By contrast, the "flatter" load profiles associated with the Peak Demand and Weighted Sum MPC systems have some flexibility to compensate for the sharp drop in the on-site solar generation (although to a small degree) when it occurs.

The contrasting behaviors help shed some light on some of the inherent limitations associated with the Net Energy Use MPC in mitigating grid impact. As can be seen from Figures 5 and 11, this MPC scheme results in a significant ramp up of the load prior to the solar outage event during the "high solar" day when both perfect and imperfect forecasting are considered. As might be expected, the ramp up is noticeably more pronounced under imperfect forecasting conditions. It should finally be noted that none of the supervisory MPC strategies considered place penalties on the sharp rise in building load (penalties are imposed only on the peak values). Such sharp ramps, however, are typically problematic for grid operations.

4.3.2. Implementation during a "Low Solar" Day

To evaluate the performance of the supervisory MPC strategies under a variety of conditions, we consider in this part the implementation of the MPC strategies and forecasting scheme on a day with low solar power availability. In this case, it is expected that the reduced accuracy of the forecast generated by the clear sky model will have a noticeable impact on the results.

Figure 12 shows the resulting profiles for the total building load under the control of the MPC strategies and the rules-based control scheme for a day where the solar power availability is quite low (and quite different from the predictions of the clear sky model). It can be seen that as solar irradiance begins its large deviation from the clear sky model prediction around 13:00, all MPC formulations appear to exhibit similarly poor responses, and appear to "collapse" onto the base case load profile. This results in the peak demand for all three MPC formulations at this initial onset of low solar generation. The qualitative differences between the different MPC formulations are not as evident in this case as they were in the case of perfect forecasting (see Figure 10) or even in the case of the "high solar" day with imperfect forecasting (see Figure 11).
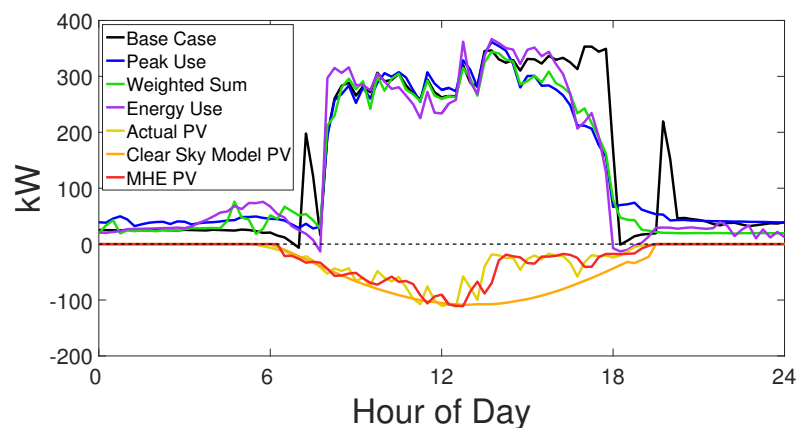

Figure 12. A comparison between the total building load profiles obtained under the rules-based control scheme (black line), the Peak Demand MPC (blue line), the Net Energy Use MPC (purple line), the Weighted Sum MPC (green line), all with a fifteen-minute moving horizon solar forecast and a five-hour MPC horizon for the "low solar" day. The actual solar power availability is shown by the yellow profile; the clear sky model's predicted solar power by the orange profile, and the estimated solar availability based on the moving horizon estimation scheme by the red profile.

It appears that, under such non-ideal conditions, all MPC formulations performed similarly, at times even approaching the performance of the rules-based case. This continues to happen until the end of the day where the building load is reduced under the MPC schemes relative to the rules-based scheme. The MPC strategies result in a more gradual ramping down of the load near the end of the day, compared with the sudden sharp load drop observed under the rules-based scheme. In terms of peak load demand, however, the MPC and rules-based schemes showed similar performance.

4.4. Quantitative Assessment of the Performance of MPC Strategies

In order to obtain a fuller picture of the differences between the different energy management strategies, the quantitative results of the simulations in terms of energy cost in dollars and peak kW usage were tabulated. This was done for both a single day, and a month-long simulated billing cycle. The supervisory MPC systems were able to outperform the rules-based scheme in every metric tabulated, regardless of whether perfect or imperfect forecasting conditions were assumed. For the perfect forecasting cases, each MPC formulation was the best performing in its respective domain; i.e., the Net Energy Use MPC resulted in the lowest energy costs across all MPC strategies, while the Peak Demand MPC produced the least peak kW usage. These trends, however, did not hold under imperfect forecasting conditions. In those instances, the performance differences between the three

MPC formulations were less predictable, and it appears like the Weighted Sum MPC would be the best choice of control and coordination scheme if just one formulation was to be selected for all types of building use.

Table 1 summarizes the results of the various test simulations on days with both high and low solar power availability under both perfect and imperfect forecasting conditions. Note that the solar power availability during the "high solar" day is very close to the availability predicted by the clear sky model, and that in the case of perfect forecasting conditions the Peak Demand MPC and Net Energy Use MPC formulations perform the best in their respective domains as mentioned previously, both for the high and low solar days, with the Weighted Sum MPC formulation striking a compromise between the two objectives. For example, for the "high solar" day, it can be seen that the Weighted Sum MPC results in a lower peak usage than the Net Energy Use MPC, and results in a lower energy usage than the Peak Demand MPC. A similar trend is observed when looking at the case of the "low solar" day. Interestingly, the peak load resulting from the Weighted Sum MPC during the "low solar" day is not substantially higher than that resulting from the Peak Demand MPC, which means that the grid impacts of the two formulations are effectively the same. This result is important because it implies that, in this case, the Weighted Sum MPC performs similarly to the optimal performance of the Peak Demand MPC (without a significant loss of optimality), while at the same outperforming it from an energy cost standpoint.

Table 1. Comparisons between the rules-based control and MPC schemes in terms of energy cost and peak load for a single day simulation, under low and high solar availabilities, and for perfect and imperfect forecasting conditions.

	Energy [$] Low Solar	Energy [$] High Solar	Peak [kW] Low Solar	Peak [kW] High Solar
Rules-Based Case	658	549	353	332
Perfect Forecast				
Peak Demand MPC	606	491	323	272
Net Energy Use MPC	569	461	356	310
Weighted Sum MPC	592	489	326	284
Moving Horizon Estimation Forecast				
Peak Demand MPC	614	507	361	296
Net Energy Use MPC	597	464	367	321
Weighted Sum MPC	585	504	344	300

The results for the imperfect forecasting scenarios show that, for the "high solar" day, the Peak Demand MPC and the Weighted Sum MPC systems perform effectively the same, with the Peak Demand MPC having a slightly lower peak load than the Weighted Sum MPC, and the latter incurring a slightly lower cost for energy usage. The Net Energy Use MPC for this case results in a larger peak load but costs the least in terms of energy. For the low solar availability case, however, it can be seen that the Weighted Sum MPC outperforms the other two formulations, both in terms of energy cost and peak demand. These results indicate that the type of weather anticipated on the day, as well as the accuracy of the forecast, should likely have an impact on the choice of the MPC strategy. Seeing as each MPC formulation appears to have its own safeguards inherently built into the way that it implements the control actions and coordinates the building subsystems.

In addition to a single day simulation, we also compared the economic performances and grid impacts of the various energy management strategies using a month-long simulation to more appropriately compare peak usage and energy costs. This comparison is particularly relevant since demand is essentially a once per month charge. The results of this comparison are shown in Table 2.

It can be seen that, as in the case of a single day simulation, all cases involving the MPC coordination strategies outperformed the rules-based control scheme for each metric. Similarly, the same trends that were observed earlier under perfect forecasting conditions continue to hold true for

the full month simulation, with the Net Energy Use MPC resulting in the lowest energy cost and the Peak Demand MPC resulting in the smallest peak load demand. For the imperfect forecasting scenario, however, the results show that of all the management schemes the Weighted Sum MPC yielded the lowest peak demand, whereas the Net Energy Use MPC resulted in the lowest energy cost. In terms of minimizing the total cost, the Net Energy Use MPC outperformed the other schemes both under perfect and imperfect forecasting conditions.

Table 2. Comparisons between the rules-based control and MPC schemes in terms of energy cost and peak load for a month-long simulation, under low and high solar availabilities, and for perfect and imperfect forecasting conditions.

	Energy [$]	Peak [kW]	Total [$]
Rule-Based Case	11,940	379	18,404
Perfect Forecast			
Peak Demand MPC	10,455	323	15,962
Net Energy Use MPC	9836	356	15,900
Weighted Sum MPC	10,431	326	15,990
Moving Horizion Estimation Forecast			
Peak Demand MPC	10,709	371	17,039
Net Energy Use MPC	9790	367	16,040
Weighted Sum MPC	10,407	349	16,354

Based on these results, it appears that the interplays between the peak demand (i.e., grid impact) and the energy use are quite subtle, with the Weighted Sum MPC scheme potentially being able to manage this on a case by case basis. It can be seen, however, that even with a rudimentary forecasting scheme such as the one used in the simulations here, the economic savings for the simulated building are appreciable.

4.5. Impact of Imperfect Forecasting

As mentioned in Section 4.3, the choice of the horizon length in the moving horizon estimation scheme has implications for the accuracy of the solar forecast. This can be seen in the comparison of the subsystem load profiles under perfect and imperfect forecasting in Figures 7 and 13, respectively.
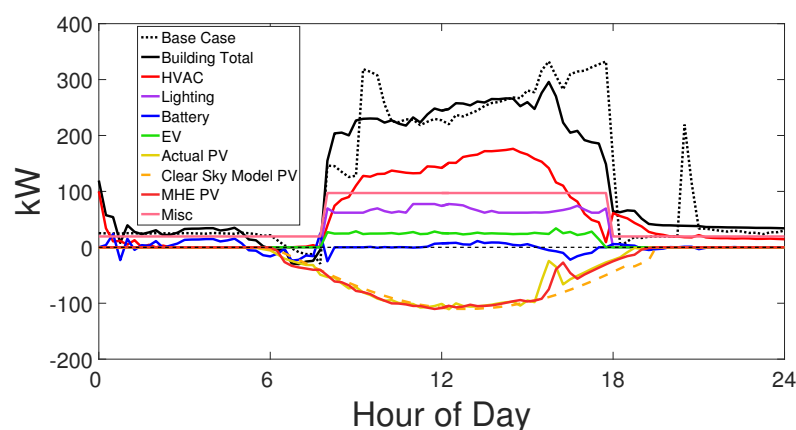

Figure 13. Power usage profiles for the entire building and the individual subsystem under the Peak Demand MPC with a fifteen-minute moving horizon solar forecast and a five-hour MPC horizon, referenced with the total building load under the rules-based control scheme.

The solar drop around 16:00 could be imagined as a cloud passing over the area. With perfect forecasting of this event in Figure 7, the loads of the individual subsystems are adjusted in anticipation of this event, resulting in no disturbance to the total building load. In Figure 13, however, the response to this "cloud" is a much more reactionary one, resulting in the subsystems operating as normal

during this reduction in solar power availability leading to the peak demand for the day at this time. This is due to the moving horizon estimation scheme using the data gathered on-site and extrapolating forward leading to an inherent limit in the time it takes to respond to changes from the internal clear sky model. This has the effect of a solar "lag" as seen in Figure 13. The estimation scheme used here is simplistic and offers reasonable results for small perturbations from an ideal clear sky day; however, there is room for improvement of this model, especially in the case of less ideal days. More advanced methods of solar forecasting may be required for more consistent cost savings to be seen.

5. Conclusions

In this work, an optimization-based approach for the management and coordination of flexible energy loads in a grid-connected commercial building with on-site solar power generation, battery storage, EV charging, controllable lighting, and HVAC system was presented. The goal of the developed approach was to simultaneously reduce the electricity cost to the user and reduce the impact of the building loads on grid operations. To achieve this goal, three objective functions—namely net energy use, peak load demand and a weighted sum of energy use and peak load—were considered in this study as surrogates to capture the financial cost to the user as well as the user's impact on the grid. Based on these surrogate objective functions, three supervisory MPC schemes that manage the local generation-load balance at the building level were developed. The supervisory MPC schemes were implemented on the simulated building with the aid of proof-of-concept models of the building subsystems together with solar forecasting schemes. The economic performance and grid impact of the MPC systems were assessed—both qualitatively and quantitatively—in relation to each other and in relation to an intelligent rules-based control strategy.

Results based on a single-day and a month-long simulation of typical weekday use indicated that the MPC schemes outperformed the rules-based control scheme with a net savings to the user and reduced strain on the grid. A quantitative assessment of the relative performances of the various energy management strategies showed that, in terms of total cost, the use of MPC schemes resulted in a net savings in the range of 7–13.6%.

Another important finding of this study was that the relative performances of the three MPC schemes is dependent on the type of weather anticipated on the day, as well as the accuracy of the forecast, which are key factors that need to be considered when choosing the appropriate MPC strategy. Specifically, under perfect forecasting conditions, it was found that each MPC formulation was the best performing in its respective domain. This trend, however, did not hold under imperfect forecasting conditions, where the performance differences between the three MPC formulations were more subtle and less predictable. Based on single-day simulations, the Weighted Sum MPC appeared to be the best choice of control and coordination scheme. However, based on the month-long simulations, it was found that the Weighted Sum MPC yielded the lowest peak demand, whereas the Net Energy Use MPC resulted in the lowest energy cost. In terms of minimizing the total cost, the Net Energy Use MPC outperformed the other schemes both under perfect and imperfect forecasting conditions.

These findings suggest that the interplays between the peak demand (i.e., grid impact) and the energy use are quite subtle, and that the Weighted Sum MPC scheme could potentially strike the necessary balance and achieve appreciable economic savings (albeit on a case by case basis), especially when accurate forecasting schemes are available.

The proposed supervisory optimization framework represents an important first step toward the inclusion of grid impact considerations in the local energy management systems for commercial and residential buildings with on-site renewable generation. This is an important and appealing goal because it enables the implementation of a more decentralized strategy for the mitigation of grid impact, which in turn creates opportunities for the wide-spread deployment and penetration of renewable energy generation sources into the grid, with all the concomitant economic and environmental benefits associated with it.

Future research work will explore the use of more complex objective functions that can better capture the notion of decentralized management of grid impact, as well as more advanced building models and solar forecasting schemes to aid in the implementation of the supervisory MPC schemes.

Conflicts of Interest: The authors declare no conflict of interest.

Appendix A. Extensible Energy Solar Load Balancing System (SLOBS) Building Model

The following is a catalog of the assumptions and equations used in the Extensible Energy Solar Load Balancing System (SLOBS) building model used in this publication. The model was compiled from the literature by Craig Wildman from Wildman Energy Consulting, LLC.

Appendix A.1. Location Data

The reference location is Merced, CA. The location data are listed in Table A1.

Table A1. Location information.

City, State	Merced, California
Latitude	37.29886 °N
Longitude	−120.5414 °E
Elevation	52 m
UTC offset	−8
Climate zone	3B [34]

Appendix A.2. Building Parameters

For modeling purposes, the following parameters in Table A2 were used for the simulated office building to size the various electrical loads, the thermal behavior, and the photovoltaic system. The building definition here is based on a "Medium Office Building" reference building, which is one of 15 reference models that NREL has developed for the DOE [34].

Table A2. DOE reference model for a "Medium Office Building".

Floor area	150,000 ft^2
Aspect ratio [(E-W length)/(N-S length)]	1.5
Number of floors	3
Floor to floor height	13 ft
Floor to ceiling height	9 ft
Glazing fraction	0.33
Occupancy rate	200 ft^2/person
Calculated total occupancy	750 people

Appendix A.3. Photovoltaic Subsystem

The rooftop solar photovoltaic plant is sized based on the roof space, and the output is estimated from the assumptions outlined in Table A3, and from the equations in [35,36]. The photovoltaic system is assumed to fit entirely inside a rectangle on the roof, and there are spaces between rows of panels too. Row spacing is assumed to be 0.5 m. The photovoltaic panel assumptions are based on a SolarWorld

panel and are intended for proof-of-concept modeling purposes. The yearly output is based on a Typical Meteorological Year (TMY) data file for Merced, CA [32].

Table A3. Photovoltaic power generation assumptions.

Roof area	4650 m^2
Total footprint (including row spacing)	75% of roof
Panel DC power at standard test conditions	290 W$_{DC}$
Efficiency at standard test conditions	17.3%
Normal operating cell temperature (NOCT)	46 °C
Cell temperature coefficient	−0.41 %/ °C
Panel length × panel width	1.67 m × 1 m
Orientation	Due south
Tilt	10°
Inverting loading ratio (max DC input/max AC output)	1.3
Inverter efficiency	96%
Calculated photovoltaic aperture area	2300 m^2
Calculated photovoltaic AC power	307 kW$_{AC}$
Calculated photovoltaic yearly output	685 MWh/yr AC
Calculated photovoltaic system capacity factor	25.5%

Standard test conditions refer to 1000 W/m^2 incident light and 25 °C temperature. Typical operating conditions frequently exhibit less lighting and higher operating temperatures.

Calculation of the incident light on the solar plant output at a given hour of the year takes into account the orientation of the panel, sun position, the direct normal irradiance, and diffuse irradiance of the TMY file at that hour, and the reflectivity of the roof surface around the panels. The performance of the solar system is then taken into account to find the AC power output at every hour of the year, and the output is summed to find the yearly output. The reader is referred to Chapters 3 and 4 in [35] for the detailed calculations related to the sun position and incident irradiance.

Appendix A.3.1. Solar Photovoltaic Output

The DC power output of the solar panel is calculated simply by multiplying the incident light by the stated DC efficiency, corrected by the panel temperature. First, a simple formula, as in Equation (A1), for panel temperature is used. In Equation (A1), the panel temperature is the ambient temperature $T_{ambient}$ in Celsius plus the difference between the normal operating cell temperature (NOCT) and 20 °C multiplied by the ratio of the incident irradiance and 800 W/m^2 (see page 53 in [36]).

$$T_{panel} = T_{ambient} + (\text{NOCT} - 20\,°\text{C}) \cdot \frac{I_{\text{incident}}}{800\,\frac{W}{m^2}} \tag{A1}$$

The DC power output of the solar panel is assumed for this simple model to be described by the following equation [36]:

$$W_{DC} = \eta_{DC,STC} \cdot I_{\text{incident}} \cdot (1 + (T_{panel} - 25\,°\text{C}) \cdot \tau) \cdot A_{panel} \tag{A2}$$

where T_{panel} is the panel temperature, $\eta_{DC,STC}$ is the stated panel efficiency at standard test conditions (STC), I_{incident} is the incident irradiance, τ is the cell temperature coefficient, which is the power loss as a fraction of rated power per change in temperature in units of 1/°C, and A_{panel} is the panel area.

The total AC output of the photovoltaic system is then given by the following expression:

$$W_{AC} = W_{DC} \cdot \eta_{AC/DC} \tag{A3}$$

where $\eta_{AC/DC}$ is the inverter efficiency, except that the maximum AC output is limited by the rated AC output of the inverter. Inverter size is calculated by dividing the peak DC output times the inverter

efficiency throughout the year by the inverter loading ratio (ILR). An ILR of 1.3 is realistic, meaning that the peak AC output without clipping would be 1.3 times the inverter output.

Appendix A.4. HVAC Subsystem

The HVAC system is a major electrical load in an office building. This is calculated by finding what the heating or cooling load is on the building, including treating the ventilation air, and then applying an efficiency to the HVAC system output to find the electrical input. If heating the building is required, either the electrical load is zero because natural gas is burned, or a simple efficiency of 90% can be used. If cooling is required, the refrigeration cycle efficiency is a function of the ambient air temperature. The current approach is to use an empirical correlation based on looking at data-sheets from different chiller manufacturers displayed here with ambient temperature in Kelvin.

$$\left(\text{Power draw per cooling duty,} \frac{kW, \text{electrical}}{kW, \text{thermal}} \right) = 190.1 \cdot \left(\frac{T_{ambient}}{1000} \right)^2 - 108.59 \left(\frac{T_{ambient}}{1000} \right) + 15.74 \quad \text{(A4)}$$

Appendix A.4.1. Heat Balance

The building control system may elect to heat up, cool down, or keep the temperature inside the building constant. The building heat capacity C (J/K) times the change in temperature per change in time, dT/dt, is equal to the sum of heat generation and heat transfer into the building (deemed in Figure 1 as $\dot{Q}_{environmental}$). Heat generation $\dot{Q}_{generation}$ is from people and electrical appliances, including lighting, plug loads, and elevators. The heat generated by appliances is equal to their power draw. Heat transfer through the envelope $\dot{Q}_{envelope}$ is from conduction through walls and sunlight shining through windows. $\dot{Q}_{ventilation}$ is from the fact that fresh air brought into the building must be heated or cooled to match the desired inside temperature, and heating or cooling must be used to adjust the humidity. $\dot{Q}_{HVAC}$ is the output of the building heating and cooling system, which is controllable.

$$C\frac{\Delta T}{\Delta t} \approx C\frac{dT}{dt} = \dot{Q}_{generation} + \dot{Q}_{envelope} + \dot{Q}_{ventilation} + \dot{Q}_{HVAC} \quad \text{(A5)}$$

Heat Capacity

Heat capacity is the factor that determines how fast the building heats up or cools down when the sum of heat generation and heat transfer is not zero. The assumption is currently 18 Wh/ $°C/m^2$ of total floor space, which corresponds to a heavy concrete building [37]. Note that the heat capacity will vary a great deal between types of buildings, and this factor will determine how slowly the building temperature will rise if the cooling system were turned down to manage demand, i.e., the dynamics of using the building thermal mass as a means of energy storage.

Occupancy Heat Generation

Occupancy heat generation is assumed to be 75 W/person of latent heat and 55 W/person for sensible heat for an office environment [38].

Appendix A.4.2. Envelope Heat Transfer

This section deals with the specifics of the envelope of the building, with the heat transfer calculations and formulas being based on [39]. Envelope heat transfer consists of two general paths: heat transfer through the opaque walls/roof and heat transfer through the windows. The heat balance on the exterior surfaces of the enclosure features solar irradiance, convection to the ambient air, and radiation to the environment summed and equal to conduction through the surface (i.e., a wall

or roof). The following equation is solved for all four walls and the roof and for the heat absorbed by the windows:

$$\dot{Q}_{conduction\,through\,surface} = \dot{Q}_{solar} + \dot{Q}_{convection} + \dot{Q}_{radiation} \tag{A6}$$

Conduction through Surfaces (Walls, Roof, and Windows)

The conductive heat transfer was calculated via Equation (A7).

$$\dot{Q}_{conduction\,through\,surface} = \frac{T_{exterior\,wall} - T_{interior}}{R_{conduction}} \cdot A_{surface} \tag{A7}$$

Note that there is also a convection heat transfer resistance between the air inside the building and the building interior wall. This heat transfer resistances is based on a heat transfer coefficient of 4 W/m^2/K as a rough assumption. The assumptions for the effective heat transfer coefficient (1/R) for the walls, roof, and windows are listed in Table A4.

Table A4. Assumed overall heat transfer coefficient values [34].

U walls	0.738 W/m^2/K
U roof	0.36 W/m^2/K
U windows	3 W/m^2/K

Convection to Ambient Air

We begin with the following equation:

$$\dot{Q}_{convection} = \frac{T_{ambient} - T_{exterior\,wall}}{R_{convection}} \cdot A_{surface} \tag{A8}$$

with the convective heat transfer coefficient being expressed by the following expression:

$$R_{convection} = \frac{1}{h} \tag{A9}$$

where

$$h = \frac{k \cdot Nu_L}{L} \tag{A10}$$

where Nu_L is the appropriate Nusselt number for the conditions present (free convection, forced convection or mixed convection), L is the characteristic length scale, and k is the thermal conductivity of air. The length scale for a horizontal surface like the building roof is the short side. It is the height for a vertical wall. Air properties are taken at the film temperature, which is assumed to be the average of the ambient temperature and the wall temperature. The detailed correlations for the calculation of the appropriate Nusselt number can be found in [39].

Appendix A.4.3. Radiation to the Environment

The heat transfer via radiation is expressed by the following expression:

$$\dot{Q}_{radiation} = \sigma \cdot A \cdot \epsilon \cdot \left(T_{ambient}^4 - T_{exterior\,wall}^4 \right) \tag{A11}$$

where σ is the Stefan–Boltzmann constant, A is the area exposed, and ϵ is the surface emissivity.

Appendix A.4.4. Solar Heating of Building by Absorption and Transmission

Sunlight shines on the walls and roof. The incident light on each surface is calculated in the same way as for the photovoltaic panels for each moment in time. The building is assumed to be a rectangle, to be oriented with the long walls facing East and West. The ratio of the E-W wall to the N-S wall is the aspect ratio and is listed in Table A3. The relevant assumptions are listed in Table A5.

Table A5. Roof and wall solar heating parameters.

Wall solar absorptivity	0.5
Roof solar absorptivity	0.8
Ground reflectivity	0.2

Some fraction of the sunlight incident on the windows is transmitted by it, and this is represented by the solar heat gain coefficient (SHGC), which is assumed to be 0.25 [34]. The light that is absorbed by the windows behaves like it is hitting an opaque wall. The light transmitted by the window behaves like a heat generation element inside the building.

Appendix A.4.5. Ventilation

Fresh air is inducted into the building to maintain air quality. Because the fresh air is at a different temperature and humidity, heat addition or heat dissipation is required to treat the air to maintain inside air temperature and humidity targets. The fan power required for moving air is currently neglected. A key assumption is the outside air flow, and this is assumed to be 20 cfm/person [34], and the relative humidity target is 50% [38].

The sensible heat addition $\dot{Q}_{sensible}$ is found by Equation (A12), where the mass flow of outside air $\dot{m}_{OA}$ is multiplied by the heat capacity of air C_p and the temperature difference between the outside air and the target inside air temperature.

$$\dot{Q}_{sensible} = \dot{m}_{OA} \cdot C_p \cdot (T_{outside} - T_{inside}) \tag{A12}$$

The latent heat addition from the outside air comes from adjusting the humidity. Empirical correlations are used to find the saturation pressure of water at the outside air temperature and the target inside air temperature p^*_{target}. Then the partial pressure of the water vapor in the outside air and the target inside air temperature are found from Equation (A13), where RH is relative humidity.

$$p^*_{target} = RH_{target} \cdot P_{sat\,water\,target} \tag{A13}$$

The target humidity ratio HR_{target} is found from Equation (A14), where P is the atmospheric pressure.

$$HR_{target} = 0.6121945 \cdot \frac{p^*_{target}}{P - P_{sat\,water\,target}} \tag{A14}$$

The latent heat addition to the building is found from Equation (A15).

$$\dot{Q}_{latent} = \dot{m}_{OA} \cdot (HR_{exterior} - HR_{target}) \cdot (2501 - 1.805 \cdot 0.5 \cdot (T_{interior} - T_{exterior})) \tag{A15}$$

where

$$\dot{Q}_{ventilation} = \dot{Q}_{sensible} + \dot{Q}_{latent} \tag{A16}$$

Appendix A.5. Lighting Subsystem

The building is assumed to be a modern building outfitted with LED lighting with standard illumination based on total floor space. The lighting system assumptions are given in Table A6.

Table A6. Lighting assumptions.

Target illuminance [40]	500 lux (1 lux = 1 lumen/m^2)
Luminous efficacy [41]	90 lumens/W
Calculated light power draw per area at target illumination	5.5 W/m^2
Calculated total lighting power draw at target illumination	77 kW

Appendix A.5.1. Miscellaneous Electrical Loads

The electric power draw from outlets in the building is based on an average value per floor area from the DOE reference building model, and elevators for a building of this size. Assumptions for elevator power draw are based on the DOE reference building model [34]. The assumptions for the miscellaneous electrical loads are given in Table A7.

Table A7. Electrical load assumptions.

Plug load power draw per floor area [34]	1.1 W/ft^2
Calculated total plug load power draw	165 kW
Number of elevators	2
Motor power per elevator	14.6 kW
Total elevator power draw	29.2 kW

References

1. Wang, X.; Palazoglu, A.; El-Farra, N.H. Operational optimization and demand response of hybrid renewable energy systems. *Appl. Energy* **2015**, *143*, 324–335. [CrossRef]
2. Salsbury, T.; Mhaskar, P.; Qin, S.J. Predictive control methods to improve energy efficiency and reduce demand in buildings. *Comput. Chem. Eng.* **2013**, *51*, 77–85. [CrossRef]
3. Skogestad, S.; Mhaskar, P. Energy Efficient Buildings Special Issue. *J. Process Control* **2014**, *24*, 701–1024. [CrossRef]
4. Lazos, D.; Sproul, A.B.; Kay, M. Optimisation of energy management in commercial buildings with weather forecasting inputs: A review. *Renew. Sustain. Energy Rev.* **2014**, *39*, 587–603. [CrossRef]
5. Li, X.; Wen, J. Review of building energy modeling for control and operation. *Renew. Sustain. Energy Rev.* **2014**, *37*, 517–537. [CrossRef]
6. Shaikh, P.H.; Nor, N.B.M.; Nallagownden, P.; Elamvazuthi, I.; Ibrahim, T. A review on optimized control systems for building energy and comfort management of smart sustainable buildings. *Renew. Sustain. Energy Rev.* **2014**, *34*, 409–429. [CrossRef]
7. Foucquier, A.; Robert, S.; Suard, F.; Stéphan, L.; Jay, A. State of the art in building modelling and energy performances prediction: A review. *Renew. Sustain. Energy Rev.* **2013**, *23*, 272–288. [CrossRef]
8. Verzijlbergh, R.; De Vries, L.; Dijkema, G.; Herder, P. Institutional challenges caused by the integration of renewable energy sources in the European electricity sector. *Renew. Sustain. Energy Rev.* **2017**, *75*, 660–667. [CrossRef]
9. Wang, S.; Yan, C.; Xiao, F. Quantitative energy performance assessment methods for existing buildings. *Energy Build.* **2012**, *55*, 873–888. [CrossRef]
10. Ríos-Moreno, G.; Trejo-Perea, M.; Castañeda-Miranda, R.; Hernández-Guzmán, V.; Herrera-Ruiz, G. Modelling temperature in intelligent buildings by means of autoregressive models. *Autom. Constr.* **2007**, *16*, 713–722. [CrossRef]
11. Pedersen, L. Use of different methodologies for thermal load and energy estimations in buildings including meteorological and sociological input parameters. *Renew. Sustain. Energy Rev.* **2007**, *11*, 998–1007. [CrossRef]
12. Zhao, H.; Magoulès, F. A review on the prediction of building energy consumption. *Renew. Sustain. Energy Rev.* **2012**, *16*, 3586–3592. [CrossRef]
13. Akkurt, G.; Aste, N.; Borderon, J.; Buda, A.; Calzolari, M.; Chung, D.; Costanzo, V.; Del Pero, C.; Evola, G.; Huerto-Cardenas, H.; et al. Dynamic thermal and hygrometric simulation of historical buildings: Critical factors and possible solutions. *Renew. Sustain. Energy Rev.* **2020**, *118*, 109509. [CrossRef]
14. Lucchi, E.; Dias Pereira, L.; Andreotti, M.; Malaguti, R.; Cennamo, D.; Calzolari, M.; Frighi, V. Development of a compatible, low cost and high accurate conservation remote sensing technology for the hygrothermal assessment of historic walls. *Electronics* **2019**, *8*, 643. [CrossRef]
15. Mathieu, J.L.; Price, P.N.; Kiliccote, S.; Piette, M.A. Quantifying changes in building electricity use, with application to demand response. *IEEE Trans. Smart Grid* **2011**, *2*, 507–518. [CrossRef]
16. Steinfeld, J.; Bruce, A.; Watt, M. Peak load characteristics of Sydney office buildings and policy recommendations for peak load reduction. *Energy Build.* **2011**, *43*, 2179–2187. [CrossRef]

17. Stadler, M.; Kloess, M.; Groissböck, M.; Cardoso, G.; Sharma, R.; Bozchalui, M.; Marnay, C. Electric storage in California's commercial buildings. *Appl. Energy* **2013**, *104*, 711–722. [CrossRef]

18. Kawashima, M.; Dorgan, C.E.; Mitchell, J.W. *Optimizing System Control with Load Prediction by Neural Networks for an Ice-Storage System*; American Society of Heating, Refrigerating and Air-Conditioning Engineers, Inc.: Atlanta, GA, USA, 1996.

19. Candanedo, J.; Dehkordi, V.; Stylianou, M. Model-based predictive control of an ice storage device in a building cooling system. *Appl. Energy* **2013**, *111*, 1032–1045. [CrossRef]

20. Henze, G.P.; Felsmann, C.; Knabe, G. Evaluation of optimal control for active and passive building thermal storage. *Int. J. Therm. Sci.* **2004**, *43*, 173–183. [CrossRef]

21. Zhao, P.; Suryanarayanan, S.; Simoes, M.G. An energy management system for building structures using a multi-agent decision-making control methodology. *IEEE Trans. Ind. Appl.* **2013**, *49*, 322–330. [CrossRef]

22. Oldewurtel, F.; Parisio, A.; Jones, C.N.; Gyalistras, D.; Gwerder, M.; Stauch, V.; Lehmann, B.; Morari, M. Use of model predictive control and weather forecasts for energy efficient building climate control. *Energy Build.* **2012**, *45*, 15–27. [CrossRef]

23. Lee, Y.M.; Horesh, R.; Liberti, L. Simulation and optimization of energy efficient operation of HVAC system as demand response with distributed energy resources. In Proceedings of the 2015 Winter Simulation Conference (WSC), Huntington Beach, CA, USA , 6–9 December 2015; pp. 991–999.

24. Zavala, V.M. Real-time optimization strategies for building systems. *Ind. Eng. Chem. Res.* **2013**, *52*, 3137–3150. [CrossRef]

25. Aswani, A.; Master, N.; Taneja, J.; Krioukov, A.; Culler, D.; Tomlin, C. Energy-efficient building HVAC control using hybrid system LBMPC. *IFAC Proc. Vol.* **2012**, *45*, 496–501. [CrossRef]

26. Hu, J.; Karava, P. Model predictive control strategies for buildings with mixed-mode cooling. *Build. Environ.* **2014**, *71*, 233–244. [CrossRef]

27. Cho, H.; Luck, R.; Eksioglu, S.D.; Chamra, L.M. Cost-optimized real-time operation of CHP systems. *Energy Build.* **2009**, *41*, 445–451. [CrossRef]

28. Hammons, T. Integrating renewable energy sources into European grids. *Int. J. Electr. Power Energy Syst.* **2008**, *30*, 462–475. [CrossRef]

29. Yan, Y.; Qian, Y.; Sharif, H.; Tipper, D. A survey on smart grid communication infrastructures: motivations, requirements and challenges. *IEEE Commun. Surv. Tutor.* **2013**, *15*, 5–20. [CrossRef]

30. Pacific Gas and Electric Tariffs. Commercial Rates Effective 1 October 2016, A-10 TOU Rate, Table B. Available online: https://www.pge.com/tariffs/electric.shtml (accessed on 15 June 2020).

31. Diamond, H.J. U.S. Climate Reference Network after One Decade of Operations: Status and Assessment. *Bull. Am. Meteorol. Soc.* **2013**, *94*, 489–498. [CrossRef]

32. National Oceanic and Atmospheric Administration; National Centers for Environmental Information. U.S. Climate Reference Network. Merced, CA Site Data. Available online: https://www.ncdc.noaa.gov/crn/ (accessed on 15 June 2020).

33. Stine, W.; Harrigan, R. *Solar Energy Systems Design*; John Wiley and Sons, Inc.: Hoboken, NJ, USA, 1986.

34. Deru, M.; Field, K.; Studer, D.; Benne, K.; Griffith, B.; Torcellini, P.; Liu, B.; Halverson, M.; Winiarski, D.; Rosenberg, M.; et al. *U.S. Department of Energy Commercial Reference Building Models of the National Building Stock*; UNLV: Las Vegas, NV, USA, 2011.

35. Stien, W.; Geyer, M. Power from the Sun. Available online: http://www.powerfromthesun.net/book.html (accessed on 1 January 2001).

36. Messenger, R.; Ventre, J. *Photovoltaic Systems Engineering*; CRC Press: Boca Raton, FL, USA, 2010.

37. Braun, J. Load Control Using Building Thermal Mass. *J. Sol. Energy Eng. Trans. ASME* **2003**, *125*. [CrossRef]

38. American Society of Heating, Refrigerating and Air-Conditioning Engineers. *ASHRAE Handbook-Fundamentals*; W. Stephen Comstock: Atlanta, GA, USA, 2013.

39. Mills, A. *Heat Transfer*; Prentice Hall: Upper Saddle River, NJ, USA, 1999.

40. US General Services Administration. 2003 Facilities Standards (P100): 6.15 Lighting. Available online: https://www.gsa.gov/node/82715 (accessed on 15 June 2020).

41. DOE Office of Energy Efficiency & Renewable Energy. LED Basics. Available online: https://www.energy.gov/eere/ssl/led-basics (accessed on 15 June 2020).